MICROWAVE EMISSION FROM PULSED, RELATIVISTIC e-BEAM DIODES

II. THE MULTIRESONATOR MAGNETRON

by

A. Palevsky and G. Bekefi

Preprint PFC/JA-78-5

Plasma Research Report

PRR 78/32
July 1978

MICROWAVE EMISSION FROM PULSED, RELATIVISTIC e-BEAM DIODES*

II. THE MULTIRESONATOR MAGNETRON

by

A. Palevsky and G. Bekefi

Department of Physics and Research Laboratory of Electronics

Massachusetts Institute of Technology

Cambridge, Massachusetts 02139

Abstract

The design and operating characteristics of relativistic, electron beam magnetrons are described. The magnetrons are comprised of a pulsed field-emission cathode (~360kV, ~15kA, ~30nsec) and several coupled resonators embedded in the anode block. The tubes are designed to work at fixed frequency, in range from 2.3 to 5GHz. The peak powers generated are typically 500 to 1000MW.

---

*This work was supported by the Air Force Office of Scientific Research (Grant AFOSR77-3143).

1. INTRODUCTION

The magnetron has long been known[1,2] to be one of the most efficient and rugged devices for generating microwaves at decimeter and centimeter wavelength ranges. Power levels from tens of watts to hundreds of kilowatts can be achieved with conversion efficiencies as high as 80 percent. In recent years[3-9] a new class of pulsed magnetron devices came into existence capable of extending the existing powers by more than two orders in magnitude. This has resulted in the generation of unprecedented powers in the range of hundreds of megawatts to several gigawatts, (albeit at reduced efficiences of 10-35 percent). The advance rests on the development, within the last decade, of high voltage pulsed power sources[10] which are being utilized to energize these novel microwave tubes.

In conventional magnetrons,[1,2] voltages of a few hundred volts to several tens of kilovolts are applied between the anode block and a heated, thermionic cathode (Fig. 1). Typical currents drawn from the cathode by a combination of thermionic emission and secondary emission[11] by back-bombardment of the cathode do not exceed a few hundred amperes. In contrast, the magnetrons discussed in this paper are furnished with cold, field emission graphite cathodes capable of delivering as much as 100 kA of current. This is achieved by applying voltages[3,5] of 200-600 kV across millimeter wide vacuum gaps separating the anode from the cathode. As described elsewhere,[12,13] this pulsed power is supplied by the "NEREUS" high voltage machine capable of delivering to a 4 ohm matched load 1.3 kJ of e-beam energy at 600 kV maximum, for a period of 30 nsec.

We observe that in order to obtain the aforementioned levels of field emission, the anode-cathode gap $d = (r_a - r_c)$ is necessarily small (several millimeters), the maximum value depending on the cathode material, surface smoothness, and the applied voltage available[14] (for a

smooth graphite surface $V/d \gtrsim 500$ kV/cm). Thus, in our magnetrons the quantity d/r_a is in the range from 0.15 to 0.25 and the geometry approaches that of the so-called[13] "planar magnetron". On the other hand, conventional low voltage, low current tubes operate in the regime $d/r_a \gtrsim 0.5$. This difference can be quite significant in the design of the magnetron, because, as we shall see later, the configuration of the rf electric field in the gap is quite sensitive to the value of d.

Table 1 summarizes some of the design characteristics of several magnetrons constructed by us. The main geometrical parameters of interest are the cathode radius r_c; the inside radius of the anode block r_a; the radius r_v of the vane-type resonator used; the angle ψ subtended by the resonators on axis; the number N of resonators, and the length L of the anode block. In all cases studied, the cathodes are machined from solid, dense graphite blocks (POCO Graphite™). The anodes are made from aluminum, oxygen-free copper or tellurium copper. The last named is preferred by us because it is more readily machined than copper.

The power from the magnetrons listed in Table 1 is coupled out into a section of rectangular waveguide via a single capacitive window cut in one of the resonators. Thus, the radiation leaves the system in the TE_{01} mode of a rectangular output guide.

2. DESIGN CRITERIA

(a) Magnetic Field and Voltage Characteristics

As in the smooth-bore magnetron described in a previous publication[13] (henceforth called paper I), the multiresonator magnetron comprises a cylindrical anode of radius r_a enclosing a coaxial cylindrical cathode of a radius r_c as is illustrated in Fig. 1. The electrons emitted by the cathode are subjected simultaneously to a uniform quasi-steady axial magnetic field B_z, and an almost radial, quasi-steady electric field

$E_r(r)$ generated by applying voltage V between the two electrodes. And, just like in the smooth-bore magnetron, the onset of an azimuthally rotating Brillouin space-charge cloud requires that B_z exceed the critical magnetic field B* given by the "Hull criterion",[13]

$$B^* = (m_o c/ed_e)[\gamma_o^2 - 1]^{1/2} \quad \text{Tesla} \tag{1}$$

where

$$\gamma_o = (1 + eV^*/m_o c^2);\ d_e = (r_a^2 - r_c^2)/2r_a, \tag{2}$$

and m_o and e are the rest mass and charge of an electron, respectively; V=V* is the diode operating voltage when B_z=B*.

The resonators cut in the anode block (and they can be of many shapes[1]) are of crucial importance. In their absence, as in the case of the smooth-bore magnetron, the electromagnetic modes in the smooth annular gap can be decomposed into rotating waves whose phase velocities are always greater than the speed of light c (note that the gap or "interaction-space" as it is often called is in fact a cavity resonator and the dispersion characteristics are in reality those of an infinite set of discrete modes rather than waves of continuously variable frequency, as will be seen below). But, in the presence of periodically spaced cavities, a certain set of modes excited in the interaction space have phase velocities less than c. Thus, when phase synchronism is established between any one of these modes n and the sheared space charge (see paper I) drifting with velocity $v_\theta = E_r(r)/B_z$, strong wave-particle interaction sets in, resulting in efficient conversion of beam energy to electromagnetic energy. This is quite unlike the smooth-bore system wherein such synchronism cannot be established and where, consequently, the coupling of energy into a given mode is found to be inefficient.[13]

It is now clear that as B_z is gradually increased beyond B* (at,

say, constant V) the space charge drift velocity will slow down sufficiently until, the outermost electron layers comprising the sheared space-charge cannot move in synchronism with the given mode n. Strong oscillations will then cease. The magnetic field $B_z=B_{BH}$ at which this happens is determined from the Buneman-Hartree condition.[15] Its relativistically correct statement[16] is

$$eV_{BH}/m_oc^2 = (eB_{BH}\omega_n/2m_oc^2n)(r_a^2 - r_c^2) - \{1 - [1 - (r_a\omega_n/cn)^2]^{1/2}\} \qquad (3)$$

where ω_n is the oscillation frequency of a given azimuthal mode of mode number n (n=1,2,3 ...), and V_{BH} is the diode operating voltage, $V=V_{BH}$, corresponding to the magnetic field $B_z=B_{BH}$.

We have seen that strong magnetron oscillations can be expected only when the magnetron operates within the limits prescribed by the Hull and the Buneman-Hartree criteria, namely when

$$B^*(V^*) \leq B_z \leq B_{BH}(V_{BH}) \qquad (4)$$

This has been confirmed experimentally as is illustrated in Fig. 2. The two solid lines are from Eqs. 1 and 3 and the dashed line represents the operating range of our 6 resonator magnetron A6 (see Table 1). The solid dot gives the magnetic field B_z and voltage V at peak operating power. Observe that the magnetron oscillates in mode n=6. When the anode number n is changed a different straight line tangent to the Hull parabola is generated. As n increases at fixed ω the slope of the straight line decreases. Conversely, as ω is increased at fixed n, the slopes of the Buneman-Hartree lines increase. It is clear from the foregoing discussion that Eqs. 1 through 4 are very useful tools in magnetron design. The following subsection is concerned in the calculations of the frequencies ω_n which must, of course, be consistent with the requirements of Eq. 4.

(b) Dispersion Characteristics

The annular interaction space $d=r_a-r_c$ together with the periodically spaced cavities can be viewed as a coaxial microwave resonator of complicated geometrical cross section. Or it can be viewed as a coaxial transmission line operating at a frequency equal to the cutoff frequency. The modes of interest which this resonator supports belong to the family of transverse electric modes (TE or H modes), with the rf magnetic field lying entirely along the z axis. To compute the frequencies of the natural modes of oscillation we solve Maxwell's equations under two assumptions. First, we assume that the cathode and anode are infinitely long along the z axis, thus making the problem entirely two dimensional; and secondly, we assume that the electron space-charge which normally occupies part of the interaction space d is absent. The justification for both assumptions will be given later in this subsection.

One then solves[17] Maxwell's field equations in vacuum for the interaction space alone, and for the anode-block resonators alone. Setting the rf admittance (or the average Poynting flux) of one equal to the rf admittance of the other over their common interface leads to a transcendental equation for the desired frequencies ω_n. In Fig. 3 are shown plots of these computer generated admittances as a function of frequency, for our A6 (N=6) six-vane magnetron. The points of intersection give ω_n. There is an infinite number of resonances, but only the lowest few $n \leq N$ are of interest. A more revealing way of presenting this data is illustrated in Fig. 4 in the form of a Brillouin dispersion diagram. The system is seen to be highly dispersive: as n and thus the phase angle increase, the phase velocity (given by the slope of a straight line drawn from the origin) decreases. The mode labelled $n=N/2=3$ is the so-called "π-mode" for which most conventional magnetrons are designed.

For this mode the rf electric fields in adjacent resonators are 180° out of phase with one another. Our magnetrons oscillate preferentially in n=N=6 or the "2π-mode" (also called[1] the 0_1 mode) which is characterized by the fact that the rf fields of all resonators are precisely in phase. Observe that the phase velocities for the n=3 and n=6 modes happen to be the same. But this fact appears to be purely coincidental and occurs for the A6 and B6 magnetrons only (see Table 1). This degeneracy can be removed by changing r_v and ψ of Table 1.

The computed frequencies and the phases are checked experimentally by a series of "cold tests" carried out as follows. The magnetron anode is placed on a test bench together with a dummy metal cathode. A tiny probing antenna is embedded in the cathode and is allowed to project slightly within the interaction space. The entire cathode assembly can be rotated about the z axis. A weak microwave signal is injected into one of the anode-block resonators, and is detected by the probing antenna. The transmitter frequency is then swept from 2 to 5 GHz and the resonant frequencies measured. Table 2 compares the measured and calculated frequencies. The agreement is seen to be good, showing that our assumption of an infinitely long anode block is not serious. However, this is not too surprising since the physical length L of our anode is 7.2 cm and is roughly equal the free space wavelength λ. For shorter anodes as those used in conventional magnetrons[1] where $L/\lambda \approx 0.25$, the differences[18] become significant. In general, the shorter the length L of the anode block the shorter is the wavelength λ_n compared with that computed for $L \to \infty$. We have comfirmed this fact by comparing the frequencies of the A6 and B6 magnetrons which differ from one another in length only.

The phases of adjacent resonators are tested by rotating the cathode and its probing antenna, and determining the phase of the received signal

interferometrically for the mode n in question.

It is important to note that in our magnetrons the various modes are well separated in frequency. As the number of resonators increases, the frequency separation decreases; multimoding, unstable operation, and overall deterioration in performance sets in. For more than eight resonators, one must generally resort to magnetron strapping,[19] rising sun resonator configuration,[20] or to coaxial resonator configuration.[21] Each of these alternatives brings with it its own difficulties, including such problems as arcing or rf breakdown at the field levels in question. Therefore, in these early stages of design, when detailed performances and questions of materials are still lacking, we purposely avoided the more complex anode block configurations. Undoubtedly much will be learned from the next generation devices which incorporate these ideas.[22]

In addition to the principal resonances discussed above, cold tests disclose a series of unwanted resonances ω_n' associated with the finite length L of the resonator system. The frequencies of these "axial modes" depend sensitively on boundary conditions at the ends of the anode block such as whether the ends are electrically open or closed (or in-between). All our magnetrons are provided with removable metal end-caps and by removing one end-cap, or both, allows us to test magnetron performance as a function of axial boundary conditions. The frequencies of the axial modes are approximately given by[23]

$$\omega_n'^2 = \omega_n^2 + (n\pi c/2L)^2 \quad , \qquad n = 0,1,2,3 \ldots \quad (5)$$

We have measured the axial variation of the electric field amplitude of several axial modes by moving the probing antenna embedded in the cathode axially, along its length. Only when the anode has end-caps do the modes show well-defined nodes in the electric field. With open ends the anti-

nodes do not always coincide with the end of the anode and their position depends on the proximity of other metal surfaces. Then L of Eq. (5) must be replaced by an effective length L_{eff}. We find, typically, that $L_{eff} \simeq 1.2L$.

In the presence of axial modes, multimoding in the magnetron cannot be ruled out. To minimize its occurrence it is necessary that no two modes lie on the same or on a nearby Buneman-Hartree curve (said differently, the phase velocities of the neighboring modes must be well-separated). As is seen from Eq. (3), this requires that the quantities ω_n'/n and ω_n/n of all modes be as far removed as possible from the quantity ω_n/n of the mode for which the magnetron is designed. (The fact that this criterion is not met in the A6 magnetron for the modes n=3 and n=6 will be discussed in the next subsection.)

We have seen that the calculated frequencies ω_n are in satisfactory agreement with cold tests. Are the calculations still meaningful under operating conditions, when a portion of the interaction space is filled with the dense electron space-charge cloud and when it may well contain some cathode and anode plasma[12] as well? Here the answer is less certain; but we believe from our frequency measurement of the n=6 mode and from some measurements on the n=3 mode, both made under operating conditions, that the mode frequencies are not significantly changed by the presence of the space-charge cloud (see Table 2).

(c) RF Electric Field Configuration

One of the most characteristic properties of a fully oscillating magnetron is the formation of rotating space-charge "spokes"[24,25,26] from the initially smooth unperturbed flow. The spokes extend from cathode to anode and they rotate with a speed close to the phase speed of the mode in question. Spoke formation is a direct consequence of the adiabaticity

of the electron motion. The frequency ω_n/n in the rotating wave frame is small compared with the cyclotron frequency, and the principal motion of the electrons is therefore an $\vec{E}\times\vec{B}_z/B_z^2$ drift in the <u>combined</u> dc and rf electric fields. In other words, the electrons move predominantly along instantaneous equipotential lines; they also execute small, second-order gyro-oscillations about them.

Whether or not a given mode is condusive to strong spoke formation (and thus to efficient magnetron oscillations) depends on the configuration of its rf electric field. The purpose of this subsection is to examine the fields of the "π mode" (n=3) and the "2π mode" (n=6) of our six cavity magnetron and then draw qualitative conclusions from the respective comparisons. To this end we will assume (to the lowest degree of approximation) that the rf fields are unchanged by the presence of the space charge. This may not be too harsh an assumption at least in the vacuum region between the anode $r=r_a$ and the original surface of the Brillouin cloud $r=r_o$ (see paper I) before spoke formation took place.

A solution of Maxwell's equations in the empty interaction space $d=r_a-r_c$ is readily performed[17] and the computer generated results are illustrated in Fig. 5. The diagrams represent the electric field lines for modes n=3 and n=6. Good spoke formation requires an "equal mix" of radial and azimuthal field components. It is seen that the n=6 mode is likely to be somewhat better in forming spokes than the n=3 mode. This may well be the reason why in our experiments much more power is achieved in the former than in the latter. Interestingly, exactly the reverse situation occurs in conventional magnetrons. Figure 6 shows our computations for the familiar[1] ten vane high power HP10V tube. This tube is normally strapped but in our computations we neglect strapping since it is not really relevant to the present discussion. We see in Fig. 6 that now the

π-mode (n=N/2=5) is probably very efficient in forming spokes but the 2π-mode (n=10) does poorly. In addition, the rather strong azimuthal field, associated with the 2π-mode, midway between the resonators tends to cause a dephasing every half period. The reason is obvious from the electric field plots which show that the n=10 mode has strong azimuthal field component but rather weak radial electric fields. The n=5 mode, on the other hand, has well-developed field components along both directions. These facts tend to substantiate the lack of success[27] of operating conventional magnetrons in the "2π-mode". However, 2π-mode operation may well be an advantage since, as is seen from Figs. 3 and 4, this mode is well-separated from the others.

The differences in the field configurations of a given mode n in the relativistic magnetron and a conventional magnetron come from differences in the gap widths d. Our relativistic magnetrons have smaller gaps than typical conventional magnetrons. For example, we see from Figs. 5 and 6 that our tube A6 has a gap approximately one-half that of HP10V tube. As a result of the proximity of the metal electrodes, the azimuthal electric fields in the A6 tube tend to be "shorted out", thus weakening the azimuthal compared with the radial electric field components. To obtain comparable gap widths in the two types of tubes, and thus cause them to operate under similar conditions, the relativistic magnetron needs to be operated at higher potentials than are available to us, typically at 600-1200kV. At these potentials sufficient field emission will take place[14] with gaps 1 to 2cm in width.

The magnitudes of the rf electric and rf magnetic fields permissible in a practical device are governed by several considerations. The rf electric field is limited by breakdown even for good vacua (pressure $\lesssim 10^{-4}$ Torr). One cause of breakdown comes about through the evolution of

impurity gases from metal surfaces, leading to the formation of cathode and anode plasmas.[12] Another comes from secondary electron emission at the surfaces leading to multipacting.[28] Fortunately, the occurrence of breakdown within the magnetron is lessened by the presence of the strong axial dc magnetic field.[29]

Limits on the maximum rf electric field apply both to conventional and relativistic microwave generators. However, there appears to be also a limit on the maximum permissible rf magnetic field $B_z(rf)$, which is peculiar to ultra-high power relativistic devices only. If the rf magnetic field is too large, then, during one part of the rf cycle, the total magnetic field (dc plus rf) may become less than the critical magnetic field B* of Eq. (1). When this happens, the diode is no longer cutoff and electrons at the surface of the Brillouin space charge cloud traveling near the speed of light, are collected on the anode in less than half a period. To place a limit on the peak rf magnetic field we may assume that the magnetron operates at or near the d.c. field given by the Buneman-Hartree criterion (see Fig. 2). Then,

$$B_z(rf) \lesssim B_{BH} - B^* \tag{5}$$

where B* is given by Eq. (1) and B_{BH} by Eq. (3). If the magnetron operates at a lower magnetic field, as it often does (see section 3) we can write more accurately that $B_z(rf) \lesssim B_z(max) - B^*$ where now $B_z(max)$ is the magnetic field for maximum power output. Thus, for example, we find for the D6 magnetron (Fig. 12) that $B_z(max) - B^* \simeq 0.4kG$. Therefore, the peak rf magnetic field is 0.4kG, and the corresponding rf electric field is ~120kV/cm. On the other hand, for the A6 magnetron (Figs. 2 and 11) $B_z(max) - B^* = B_z(rf) \simeq 2.5kG$ and the corresponding rf electric field is ~750 kV/cm. It is noteworthy that the D6 magnetron gives consistently lower power outputs than the A6 magnetron.

Irrespective of what mechanism is operative in limiting the rf electric field, it places an upper limit on the microwave power P_{max} delivered by the device. By energy conservation,

$$P_{max} \approx \frac{\omega_n}{Q} \int_v \frac{1}{2} \varepsilon_o E^2(rf) dv \qquad (6)$$

Here P_{max} is the peak power, E(rf) is the amplitude of the electric field, v is the volume of the magnetron, and Q is the quality factor under operating conditions (that is, it is the "loaded Q" in the presence of the oscillating space charge). It is clear that high Q's and thus high electric fields are undesirable. In our magnetrons the Q's are typically in the range of 20-40.

We have raised a number of questions which in the absence of a full theoretical model can be answered only partially. Such a model does not exist either for the conventional or the relativistic magnetron. The reason is that magnetron oscillations are founded on a nonlinear instability. Better understanding will have to await detailed analysis presently underway. A two-dimensional (r, θ), fully relativistic, electromagnetic "particle in cell" computer program is being developed[30] in which Maxwell's equations are solved self-consistently in the presence of space charge. With its aid we plan to optimize magnetron design and study the relevant scaling laws with voltage, current, magnetic field, and frequency as parameters.

3. EXPERIMENTAL RESULTS

Details of the experimental setup, and techniques of measuring voltage, current, and magnetic field, etc., are identical to those described in Refs. 12 and 13. We shall, therefore, not elaborate on these topics and proceed directly to a discussion of the experimental results.

(a) Current-Voltage Characteristics

Our magnetrons are run at roughly constant diode voltage V lying in the range $V_{BH}<V<V^*$ where V^* and V_{BH} are defined in Eqs. (1) and (3) respectively. The principal variable is the axial applied magnetic field B_z. Figure 7 shows the voltage and current characteristics for the A6 magnetron measured as a function of B_z. The voltage rises slightly and the current falls fairly monotomically, results which are typical of all magnetrons tested by us. It is noteworthy that, as the magnetic field passes through its critical value $B=B^*$ ($B^*\simeq 4.9$kG for the A6 magnetron), nothing unusual takes place in the current. This is in complete variance with similar observations made on the smooth-bore magnetron.[13] In the latter, the current drops precipitously near the Hull cutoff $B_z\simeq B^*$, in accord with theoretical expectations.

One wonders whether the lack of a noticeable cutoff in a fully oscillating magnetron is due to the strong interactions of the rf fields with the electrons, causing a sizeable fraction of these to be thrown into orbits with large parallel velocities. These electrons would then move along magnetic field lines and be eventually collected on the anode (the current plotted in Fig. 7 is the <u>total</u>, radial plus axial, current). Slight misalignment or asymmetry could be another, more mundane reason for large axial currents. To test this we mount a current-viewing probe so positioned as to collect virtually all axial current. Figure 8 illustrates the results for the D6 magnetron. We see that the axial current is relatively small, and even when we subtract it from the total current, no pronounced cutoff occurs at $B_z\simeq B^*$. We thus conclude that in a cavity-loaded magnetron the wave-particle interactions are so violent that the Hull cutoff (which is a statement[13] of energy and momentum conservation in steady fields only) is largely eliminated from the current character-

istics of the device. However, the cutoff remains very much in view when one examines the rf emission characteristics, as will be shown in the next subsection.

(b) Measurements of Microwave Power

The magnetrons under test are mounted in an experimental arrangement very similar to that used in our studies of the smooth-bore magnetron.[12,13] The main difference lies in the way the rf power is being coupled out of the device. Our principal technique (but also see later) is to extract power from a single resonator, coupled via a capacitive iris to a section of tapered S-band waveguide, as is illustrated in Fig. 9a. Irises of various widths can be inserted for maximum power output. The far end of the tapered waveguide is then connected to a power measuring device. Three devices are used and the results checked against one another; the observations are found to be mutually consistent.

The one device is a modified form of calorimeter described in Ref. 31. Here, a section of evacuated waveguide is terminated in a matched resistive load, and electrically shielded thermistors measure its rise in temperature. The second device is a high power, side-wall coupled 50 db directional coupler. Most of the energy is absorbed in the matched load. A calibrated crystal detector whose output is monitored on a fast oscilloscope measures the power in the side-arm after further attenuation is provided by a precision calibrated attenuator. The entire system is either evacuated or filled with SF_6 to prevent the occurence of rf breakdown. In the third detection technique the power emanating from the waveguide passes through an evacuated, stainless-steel horn having a rectangular aperture 23cm×17cm. The radiation from the horn is picked up by a receiving antenna (a section of open waveguide) placed 3.5m from the horn. The signal is then further attenuated and detected with a calibrated

crystal detector (see also section 2 of paper I, Ref. 13). The setup is calibrated in situ to take account of antenna gains and standing waves caused by room reflections.

The voltage pulse applied across the cathode-anode gap d is roughly trapezoidal in shape with rise and fall times of ~11nsec, and a flat-topped portion of ~26nsec duration. The full width at the half-power points (FWHM) is ~38nsec. Figure 10a shows the voltage pulse and Fig. 10b the corresponding current pulse. The microwave pulse shown in Fig. 10c is substantially narrower having typical FWHM's of ~17nsec. One possible reason for the narrow microwave pulse width is rf breakdown in the magnetron, or in the associated microwave plumbing. We discard this possibility on the following grounds: we vary the magnetron output power over more than one order in magnitude with no observable change in pulse width. Rather, we ascribe the narrowness to sharp voltage tuning exhibited by the device. At fixed magnetic field B_z, there is but a narrow range of ΔV's over which the magnetron will oscillate. This explanation is confirmed by the fact that occasionally (and in particular when B_z is not optimum), two microwave spikes are observed, one occurring during the voltage rise and the other during the voltage fall, with a minimum in rf power during the plateau region in V(t). In another experiment we generate a slowly rising 300nsec voltage pulse in the form of a ramp. Microwave emission occurs only during a very short time interval of 30-40 nsec duration in which the voltage is just "right".

Figure 11 shows a plot of rf power as a function of magnetic field for the A6 magnetron. Peak power at the magnetic field of ~7.6kG equals ~0.90GW. For this device B^*=4.9kG and B_{BH}=8.8kG. We see that no significant oscillations occur at a magnetic field below cutoff $B_z \approx B^*$, and that the maximum in emission is near (but below) $B_z = B_{BH}$, in conformity with

theoretical predictions. We point out that for all our magnetrons other than A6, maximum emission occurs at somewhat lower magnetic fields with $B_z(max)$ closer to B* than to B_{BH}. Unfortunately it is at present not possible to determine from analytical considerations either the exact value of $B_z(max)$ for maximum rf power, or the expected anode current I. Needless to say, both quantities are crucial in magnetron design.

In conventional magnetrons, the cylindrical anode block is customarily open at both ends.[1] In our magnetrons we make provisions for removable metal end caps. This allows us to examine the operating characteristics of the device in the presence of one, two, or no end-caps. We find in the A6 magnetron that maximum power is achieved when both end-caps are firmly in place. Tests made on the D6 magnetron again show that more power is achieved when both end-caps are in place than when the anode block is open at both ends (no measurements were made in this magnetron with only one end-cap). The results are illustrated in Fig. 12. For a given magnetron system it is not possible to determine, a priori, the optimum end-cap configuration. It undoubtedly depends on a number of parameters, including the method of coupling out the rf power.[8,9] It is therefore advantageous to keep the options open.

Two other parameters have been varied optimizing rf power output. The first is the cathode-anode gap width. Maximum power is achieved with gaps of 5 to 6mm width. For gaps smaller than ~4mm alignment is very difficult and arcing often occurs. For gaps larger than ~7mm the anode current and thus the rf power drop significantly. Note that for a given magnetron design the gap cannot be varied at will because both B* and ω_n are quite sensitive functions of d (see section 2).

Secondly, we have varied the axial position of the cathode relative to the center of the anode block. In general rf power output can be increased by sliding the cathode axially until its free end coincides ap-

proximately with the center of the anode block. The reason is that most of the current is emitted from the free 1cm long section of our 4.0cm long graphite cathode, as is confirmed by observing anode and cathode damage patterns (see Refs. 12). As a result, it is reasonable to expect maximum wave-particle interaction when the position of maximum electron emission coincides with the center of the anode-embedded resonators.

(c) Frequency Characteristics

The frequency spectrum of the emitted power is measured by means of solid state, yttrium garnett dispersive lines (Chu Associates, Harvard, Mass.) having frequency ranges from 2.0GHz to 3.1GHz and 2.8 to 4.8GHz. The received power is divided equally by means of a broad-band hybrid tee; half the signal is rectified with a calibrated crystal detector and displayed on a fast oscilloscope. The other half passes through the dispersive line, solid state amplifier (Avantek) and a tunnel diode detector (Aerteck). The signal from the detector is likewise displayed on the aforementioned oscilloscope. The time delay between the dispersed and undispersed (reference) signals is nearly lineraly proportional to the frequency of the radiation. Typical results are shown in Fig. 13a. The clean, single-spiked dispersed signal signifies that the magnetron oscillates predominantly at a single frequency. We cannot determine the precise line width of the resonant mode using this technique. However, we place an upper limit of 40MHz on its width.

The results of Fig. 13a are for the case when the magnetic field $B_z \equiv B_z(\max)$ is adjusted for maximum power output. Clean, single mode behavior persists even when $B_z > B_z(\max)$; however, for low magnetic fields $B^* \lesssim B_z \lesssim B_z(\max)$, the dispersed signal becomes spiky, suggesting that mode-breakup is taking place. This is illustrated in Fig. 13b. Alternately, multimoding can occur as is shown in Fig. 13c. At very low magnetic

fields $B_z \simeq B^*$ the magnetron oscillations tend to jump into an entirely different frequency regime as will be discussed momentarily.

The frequency of oscillation of Fig. 13a corresponds to the "2π-mode" (n=N=6) as was mentioned already in section 2. The frequency f≃4.6GHz. Maximum power output is achieved in this mode. As the magnetic field is reduced from B_z(max) and B* is approached, the oscillation frequency drops suddenly to a new value of f≃2.3GHz. We believe that we are now witnessing oscillations in the "π-mode" (n=N/2=3). The frequency spectrum is quite clean but the emitted power is at best an order of magnitude lower than it is for the n=6 mode.

In section 2 we give tentative reasons for 2π versus π-mode operation. Another possible reason for "quenching" of the π-mode is the asymmetric manner in which power is extracted from the magnetron (Fig. 9a). Since only one resonator is loaded, and it is loaded heavily, π-mode symmetry may be partially destroyed. By narrowing the width of the coupling iris, the requisite symmetry can be restored. Nonetheless, we find no enhancement in the intensity of π-mode radiation. (The iris can be narrowed down up to a point; for gaps that are too narrow, there is evidence of rf breakdown.)

In another experiment the emission from the A6 (and D6) magnetron is coupled out symmetrically by allowing the radiation to escape in <u>equal amounts</u> from each resonant cavity. The emitted radiation is then allowed to fill a section of cylindrical waveguide 17cm in diameter surrounding the anode block (see Fig. 9b). The radiation ultimately leaves the system axially via a 17cm plexiglass window. This manner of coupling leads to excitation of the $TE_{01}(H_{01})$ waveguide mode, and the cylindrical pipe with its output window thus behaves as a cylindrical TE_{01}-mode antenna. Despite the care taken to preserve symmetry, π-mode emission remains

weak.

In yet a third experiment, "priming" of the π-mode is attempted. The idea behind this technique is to fill the magnetron with intense radiation at the frequency of the sought-after mode, just prior to firing the main voltage source. The suitably primed magnetron is then expected to "lock onto" the required π-mode, as the voltage on the device erects. To this purpose we constructed magnetron J6 (see Table 1 and Fig. 9c) provided with two capacitive coupling irises. The one iris is for coupling out the microwave emission in our usual way; the other iris couples in 500kW of microwave power at a frequency of 2.8GHz, for a period of 2μsec. No noticeable π-mode enhancement is observed in the J6 magnetron.

On the basis of the above experiments we conclude that the lack of success in operating the relativistic magnetron in the π-mode is due to the narrow interaction gap, as was discussed in section 2.

4. DISCUSSION

The relativistic magnetron has the potential of becoming an efficient, structurally simple and rugged source of intense, pulsed microwave power in the centimeter wavelength range. Because of limitations imposed by dc and rf breakdown, it is unlikely to be useful at millimeter wavelengths where the physical distances between electrodes are small. Although our experimental tubes are energized with short, tens of nanosecond pulses, one can conceive of generators having microsecond pulse lengths. The reason is that in the magnetron geometry, the large externally applied axial magnetic field inhibits diode closure caused by motion of anode and cathode plasma.[3,12] Indeed, relativistic <u>smooth-bore</u> magnetrons have been operated for one or two microseconds.[32] From the experiments discussed in section 3 above, a good flat-topped voltage

pulse is mandatory for such long-pulse operation.

Figure 7 shows that the magnetron diode is a high impedance tube with impedances typically in the range from 20-40 ohms. Hence, for efficient operation, the pulsed voltage source should be matched to the load, unlike the situation in our experiments which employ a 4 ohm generator. Unfortunately, at the present time the matching must be made more or less empirically. Not enough is known about the magnetron to enable one to predict the tube impedance. We hope that the particle simulation code under development[30] will enable us to perform this task.

Although the relativistic magnetron is an interesting experimental tube, it has a long way to go before becoming a practical device. In particular, a serious materials study needs to be undertaken.

Graphite as cathode material has the advantage of having very good field emission characteristics[14] with one of the smallest erection delays. But, the entire diode becomes easily coated with carbon. As a result, tube performance deteriorates rapidly and the diode must be carefully cleaned after each 15-20 successive shots. Other cathode material, like aluminum, steel, or brass should be tried. If long pulse operation is contemplated, quick erection is not an issue, and molybdenum may prove satisfactory.

Anode blocks made from aluminum, copper, or tellurium copper suffer fairly severe damage. The damage occurs primarily at the resonator "teeth" and directly opposite to the free end of the emitting cathode (we recall from section 3 that electron emission is confined to the free end, and extends over 1-2cm of length only). The damage is particularly bad when the capacitor bank energizing the solenoid fails to fire and whenever $B_z < B^*$, so that the full current reaches the anode. Anyway, it is well to replace the anode block after several hundred shots. There is no appar-

ent reason why stainless steel anode blocks could not be used, and we are presently constructing one such block. As discussed in section 2, a low Q seems to be desirable, and steel with its low electrical conductivity may not be harmful.

As one proceeds to higher and higher tube voltages [5,9] and consequently to even higher tube currents, the azimuthal magnetic field B_θ generated by axial current flow[12,13] in the cathode shank, will acquire more and more importance. Suppose a current of 30kA flows; it generates an azimuthal magnetic of 4.0kG at the surface of a 1.5cm radius cathode. This field is comparable in magnitude to the externally applied axial field B_z, and may thus have a strong and undesirable influence on the space charge flow in the interaction gap. (the B_θ field crossed with the E_r field results in an axial drift of the space-charge cloud). At very large currents it may well be necessary to suppress the axial current by feeding the cathode symmetrically from opposite directions. Alternately, one can make the cathode in the form of a helical conducting ribbon as is illustrated in Fig. 14. If the pitch angle is small enough, B_θ in the interaction space can be reduced considerably. We have constructed and tested such a ribbon cathode at a current level of ~8kA, and found to our satisfaction no adverse effect in the rf performance of the tube.

REFERENCES

1. G. B. Collins, editor, "Microwave Magnetrons" (McGraw-Hill, 1948).

2. E. Okress, editor, "Crossed-Field Microwave Devices" (Academic Press 1961) Volumes 1 and 2.

3. G. Bekefi and T. J. Orzechowski, Phys. Rev. Letters 37, 379, (1976).

4. G. Bekefi and T. J. Orzechowski, Am. Phys. Soc. Bull. 21, 571 (1976), paper DM-4

5. T. J. Orzechowski, G. Bekefi, A. Palevsky, W. M. Black, S. P. Schlesinger, V. L. Granatstein, and R. K. Parker, Am. Phys. Soc. Bull. 21, 1112 (1976) papers 5G-3, 5G-4.

6. A. Palevsky, R. J. Hansman, Jr., and G. Bekefi, Am. Phys. Soc. Bull. 22, 648 (1977), paper KH-1

7. A. Palevsky and G. Bekefi, Am. Phys. Soc. Bull. 23, 588 (1978) paper GO-2

8. N. F. Kovalev, B. D. Kol'chugin, V. E. Nechaev, M. M. Ofitserov, E. I. Soluyanov and M. I. Fuks, Sov. Tech. Phys. Lett. 3(10), 430 (1977) [Pis'ma Zh. Tekh. Fiz.3, 1048 (1977)]; also V. E. Nechaev, M.I. Petelin and M. I. Fuks, Sov. Tech. Phys. Lett. 3(8), 310 (1977) [Pis'ma Zh. Tekh. Fiz. 3, 763 (1977)].

9. A. N. Didenko, A.S. Sulakshin, G. P. Fomenko, Yu. G. Shtein and Yu. G. Yushkov, Pis'ma Zh. Tekh. Fiz. 4, 10 (1978).

10. T. H. Martin, IEEE Trans. Nucl. Sci. NS-20, 289 (1973); K. R. Prestwich, IEEE Trans. Nucl. Sci. NS-22, 975 (1975).

11. R. L. Jepsen, Ref. 2, Vol. 1, page 359.

12. T. J. Orzechowski and G. Bekefi, Phys. Fluids 19, 43 (1976). Also, G. Bekefi, T. J. Orzechowski, and K. D. Bergeron, "Proceedings of the First Inernational Topical Conference on Electron Beam Research and Technology" Albuquerque, 1975, National Technical Information

Service, U. S. Dept. of Commerce UC-21, Vol. I, page 303 (1976).

13. T. J. Orzechowski and G. Bekefi, companion paper, called Paper I in text (to be published).

14. R. K. Parker, R. E. Anderson, and C. V. Duncan, J. Appl. Phys. 45, 2463 (1974).

15. O. Buneman, article in "Crossed-Field Microwave Devices" (Academic Press 1961) E. Okress editor, Vol. 1, p. 209.

16. R. V. Lovelace (private communication 1977). An equation for the planar magnetron, corresponding to Eq. 3 is given by E. Ott and R. V. Lovelace, Appl. Phys. Lett. 27, 378 (1975).

17. N. Kroll, Ref. 1, chapter 2, p. 49; also N. Kroll and W. Lamb, J. Appl. Phys. 19, 183 (1948).

18. J. C. Slater, Radiation Laboratory Report No. 43-9, August 31, 1942 Massachusetts Institute of Technology (unpublished).

19. L. R. Walker, Ref. 1, chapter 4, p. 118.

20. N. Kroll, Ref. 1, chapter 3, p. 83; also N. Kroll and W. Lamb, J. Appl. Phys. 19, 183 (1948).

21. J. Feinstein and R. J. Collier, Ref. 2, Vol.2, chapter 3, p. 123; also A. J. Bamford, W. A. Gerard, and C. H. Scullin, IEEE Trans. Electron Devices, ED-14, 844 (1967).

22. R. K. Parker is building a coaxial magnetron (private communication 1978).

23. H.A.H. Boot, H. Foster, and S. A. Self, Proc. Inst. Electr. Eng. 105 Part B Suppl. No. 10, p. 419 (1958).

24. O. Buneman, Ref. 2, Vol. 1, p. 209; S. P. Yu, G. P. Kooyers, and O. Buneman, J. Appl. Phys. 36, 2550 (1965).

25. P. L. Kapitsa, "High Power Microwave Electronics" (Pergamon Press, New York 1964). Also, J. F. Hull, Ref. 2, Vol. 1, p. 496.

26. M. Karakawa, M.S. Thesis, Department of Physics, M.I.T. 1978 (unpublished).

27. N. Kroll, Ref. 1, p. 69.

28. A. J. Hatch, Nuclear Instruments and Methods 41, 261 (1966).

29. P. F. Clancy, Microwave Journal p. 77, March 1978; B. Bischof, Nuclear Instruments and Methods 97, 81, (1971).

30. A. Palevsky, A. T. Drobot, and G. Bekefi (to be published).

31. P. Efthimion, P. R. Smith, and S. P. Schlesinger, Rev. Sci. Instr. 47, 1059 (1976).

32. S. C. Luckhardt and H. H. Fleischmann, Appl. Phys. Lett. 30, 182 (1977).

Table 1. Characteristic dimensions of several relativistic magnetrons. (The frequencies are computed for an infinitely long anode block, see section 2).

Magnetron	r_c (cm)	r_a (cm)	r_v (cm)	ψ (degrees)	N	L (cm)	f(n=3) (GHz)	f(n=6) (GHz)
A6	1.58	2.11	4.11	20	6	7.2	2.34	4.60
B6	1.58	2.11	4.11	20	6	3.81	2.34	4.60
D6	1.88	2.46	4.83	20	6	8.42	1.98	4.01
J6	1.69	2.22	3.82	18	6	7.2	2.81	5.27

Table 2. Comparison between computed and measured resonant frequencies (given in GHz) for the A6 and D6 magnetrons; "cal." means calculated values; "cold" refers to cold tests as per text; "hot" refers to measurements made when magnetron oscillates at full power. The mode nomenclature 1_o, 2_o, ... is that used in Ref. 1.

MAGNETRON \ MODE		1_o (n=1,5, ...)	2_o (n=2,4, ...)	3_o (n=3)	0_1 (n=6)	1_1 (n=1,5,..)
A6	cal.	1.35	2.12	2.34	4.60	4.97
	cold	1.54	2.17	2.41	4.55	
	hot			2.3	4.6	
D6	cal.	1.13	1.81	1.98	4.01	4.20
	cold	1.20	1.82	2.00	3.90	
	hot				3.9	

FIGURE CAPTIONS

Fig. 1. Schematic of a magnetron. The inner cylinder is the emitting cathode. The outer cylinder is the anode. There is a uniform axial magnetic field B_z pointing into the page. The region $d=r_a-r_c$, called the interaction space, is partially filled with electron space-charge rotating in the clockwise direction.

Fig. 2. The region of operation of the A6 magnetron is delineated by the two solid curves derived from Eqs. 1 and 3. The dashed line is from experiment. At the position of the solid dot the magnetron emits at maximum power.

Fig. 3. RF admittances Y computed for the A6 magnetron, as a function of frequency ω. The solid lines are the admittances of the (empty) interaction space spatially averaged over the opening to the resonators (at $r=r_a$ and $\psi/2<\theta<\psi/2$). The dashed line is the admittance of the vane-type resonators, averaged over the opening to the interaction space. The points of intersection give the oscillation frequencies. The mode nomenclature follows that adopted in Ref. 1, chapter 2.

Fig. 4. Dispersion diagram for the modes of the A6 magnetron. The slope of a straight line drawn from the origin (as for example the dashed line) gives the phase velocity of a given mode in units of segments per second.

Fig. 5. The rf electric fields of the $\pi(n=3)$ and $2\pi(n=6)$ modes of the A6 magnetron. The circular dashed line gives the outer radial boundary of the Brillouin space charge (prior to the onset of rf fluctuations).

Fig. 6. The same as Fig. 5 calculated for the HP10V tube. Note the large width $d=r_a-r_c$ of the interaction space of this tube compared with that of the A6 tube of Fig. 5.

Fig. 7. The voltage-current charcteristics of the A6 magnetron as a function of magnetic field. The current is the total radial, plus any residual, axial current.

Fig. 8. Measured total and axial currents in the D6 magnetron as a function of magnetic field. The latter is due mainly to tube misalignment and asymmetries.

Fig. 9. RF coupling circuits.

Fig. 10. Voltage, current and microwave pulse shapes. Note the small width of the microwave signal compared with that of the voltage pulse.

Fig. 11. Microwave power emitted from the A6 magnetron as a function of magnetic field. At $B_z \simeq 7.6$kG, the peak power is ~0.90GW.

Fig. 12. The effect of metal end-caps on the emission characteristics of the D6 magnetron. The solid line is for the case with end-caps, the dashed line is for no end-caps. At $B_z \simeq 4.9$kG, the peak power (with end-caps) is ~0.4GW.

Fig. 13. Spectral characteristics of the power emitted from the A6 magnetron, (a) under single mode operation, (b) in the presence of mode breakup, and (c) in the presence of multimoding. In each case the trace to the far left is the reference, undispersed, signal. On the right are the dispersed signals.

Fig. 14. Sketch of a carbon cathode machined in the form of a helical ribbon to reduce B_θ in the interaction space.

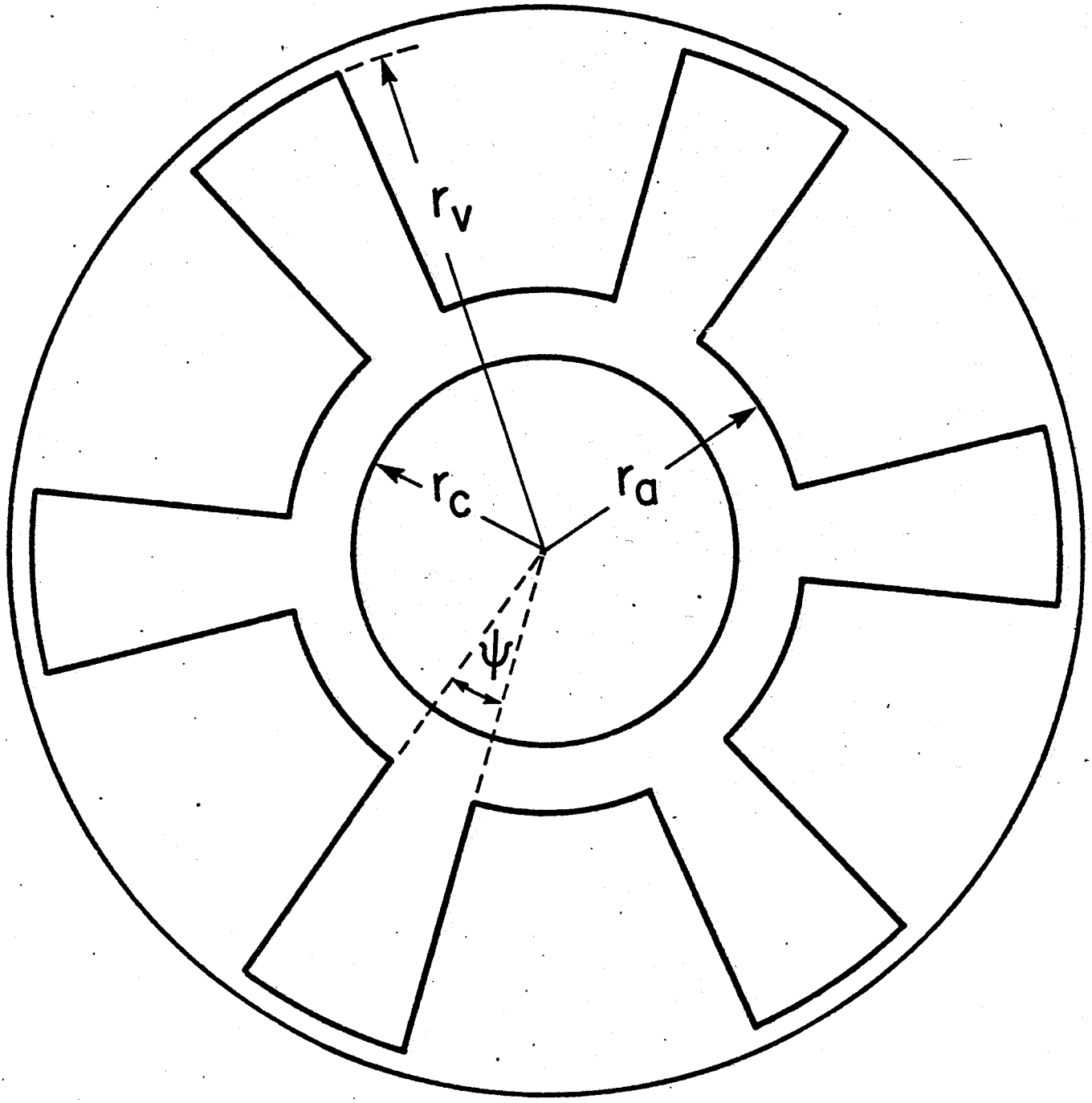

Fig. 1

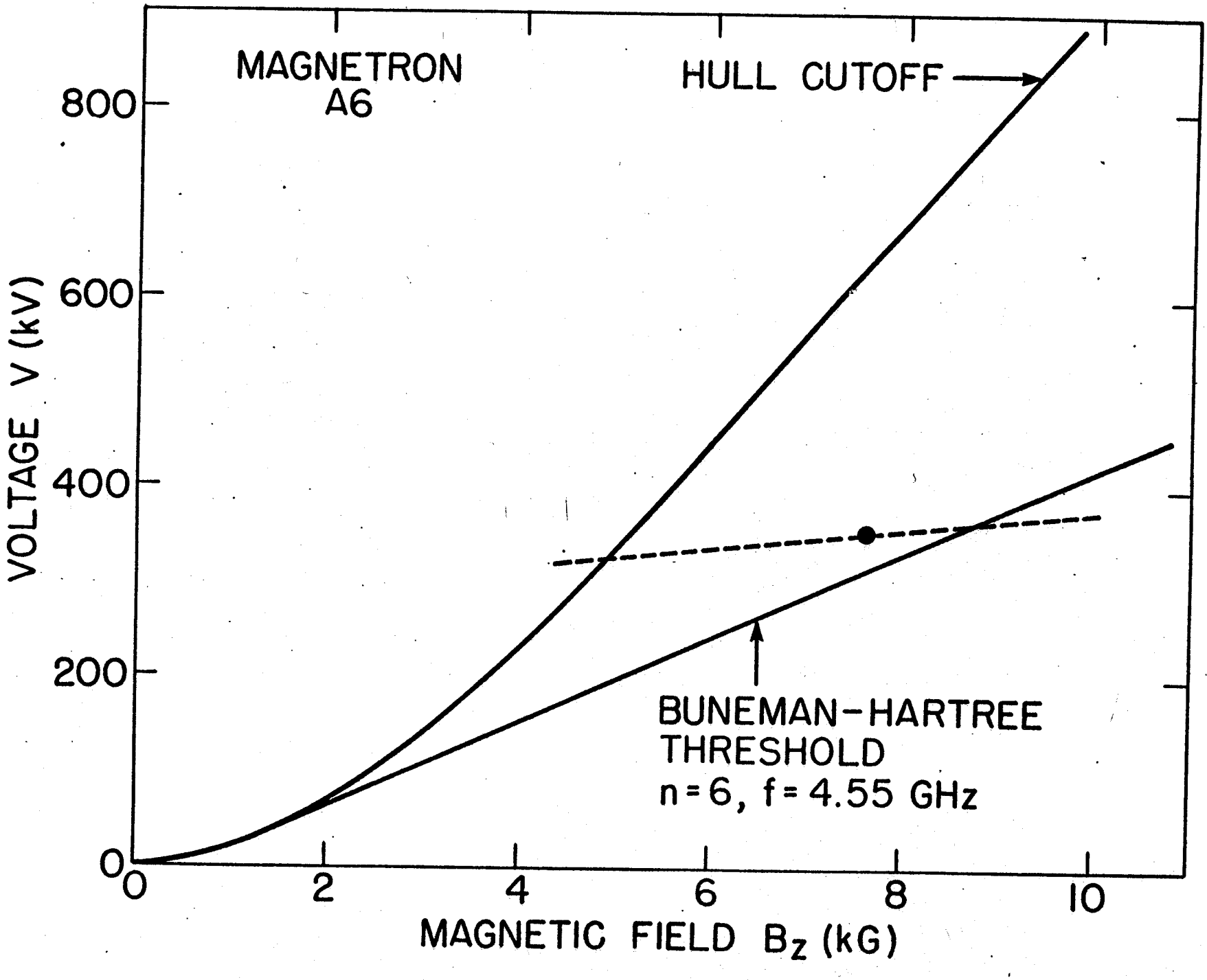

Fig.2
Palevsky and Bekefi

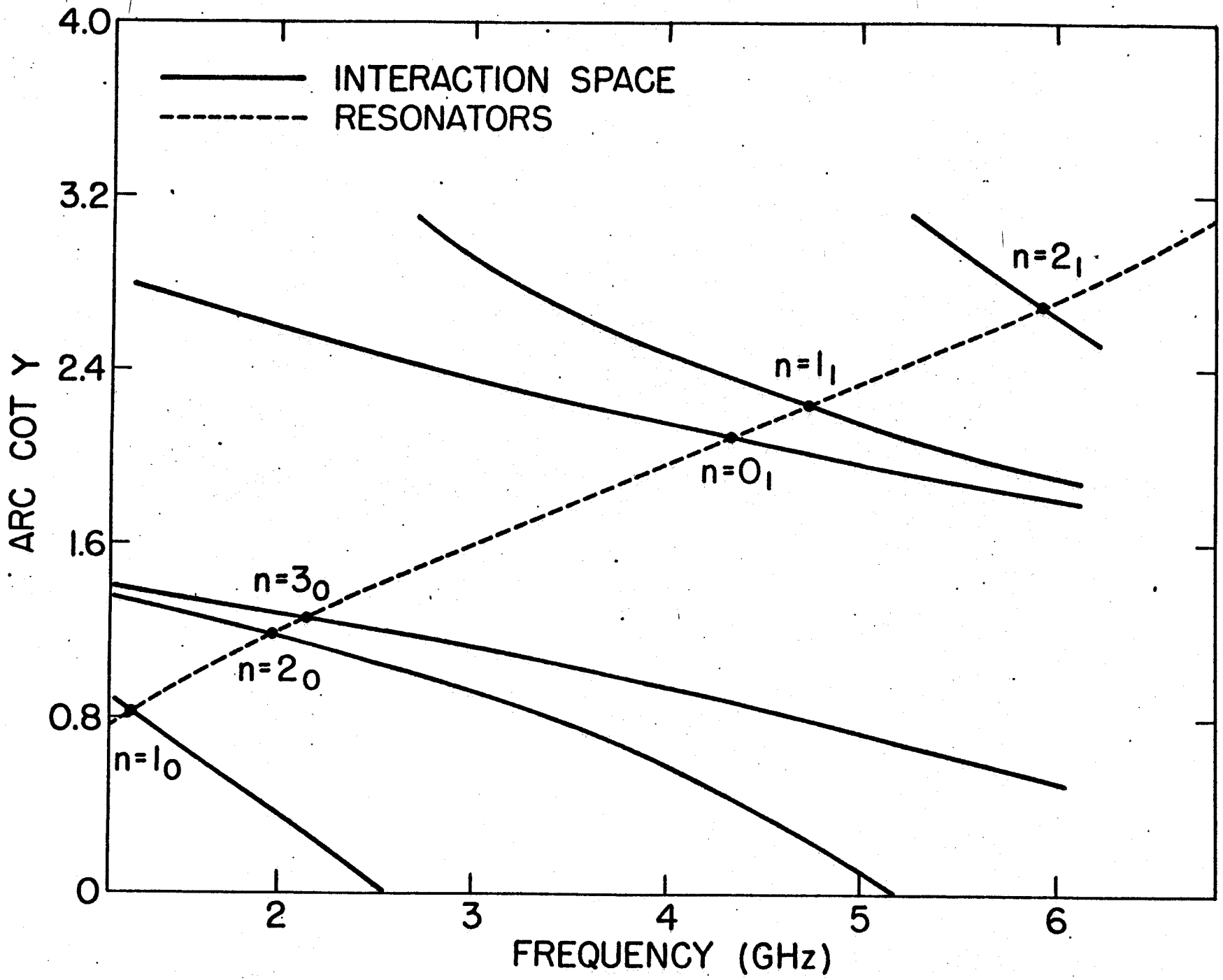

Fig.3
Palevsky and Bekefi

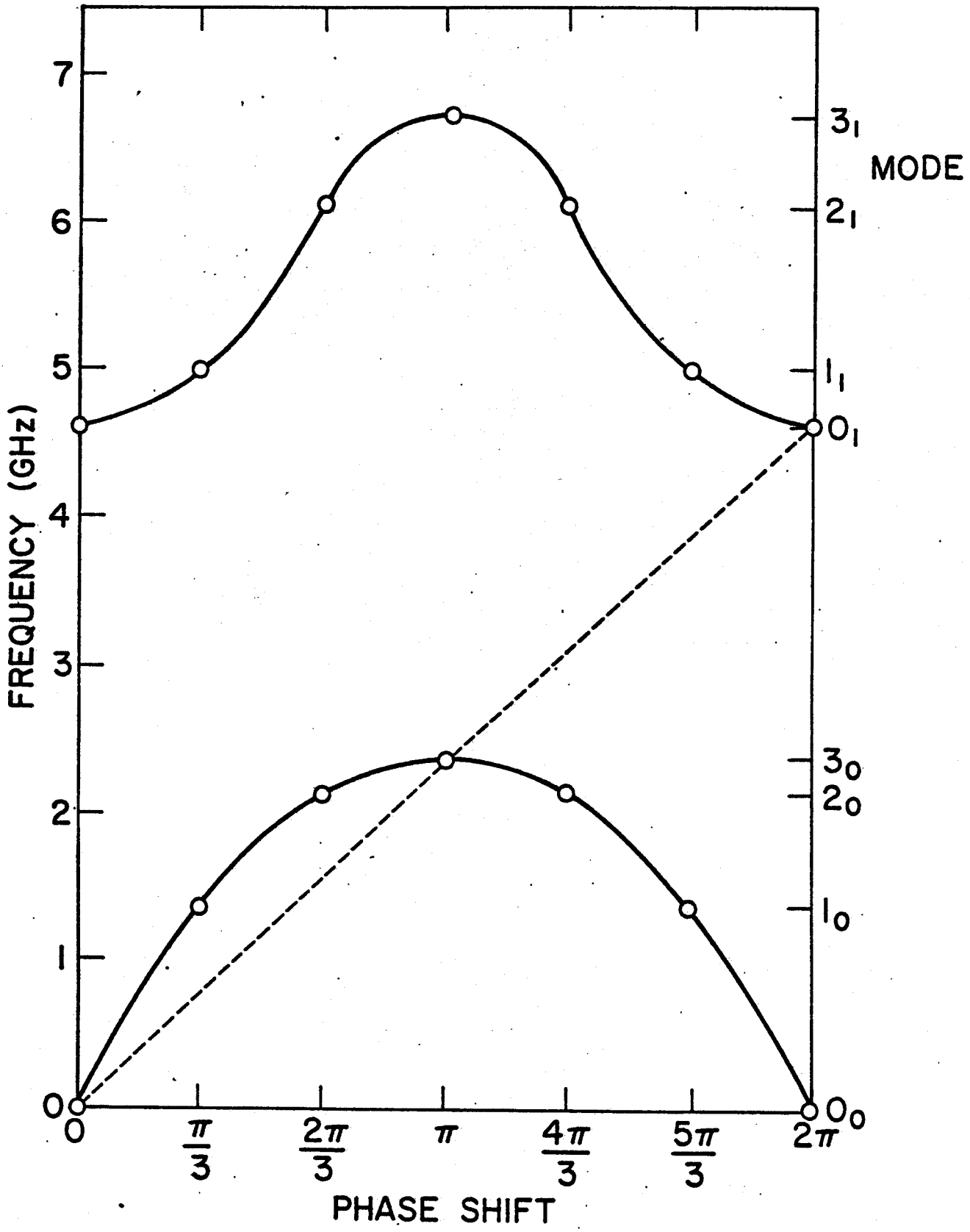

Fig.4
Palevsky and Bekefi

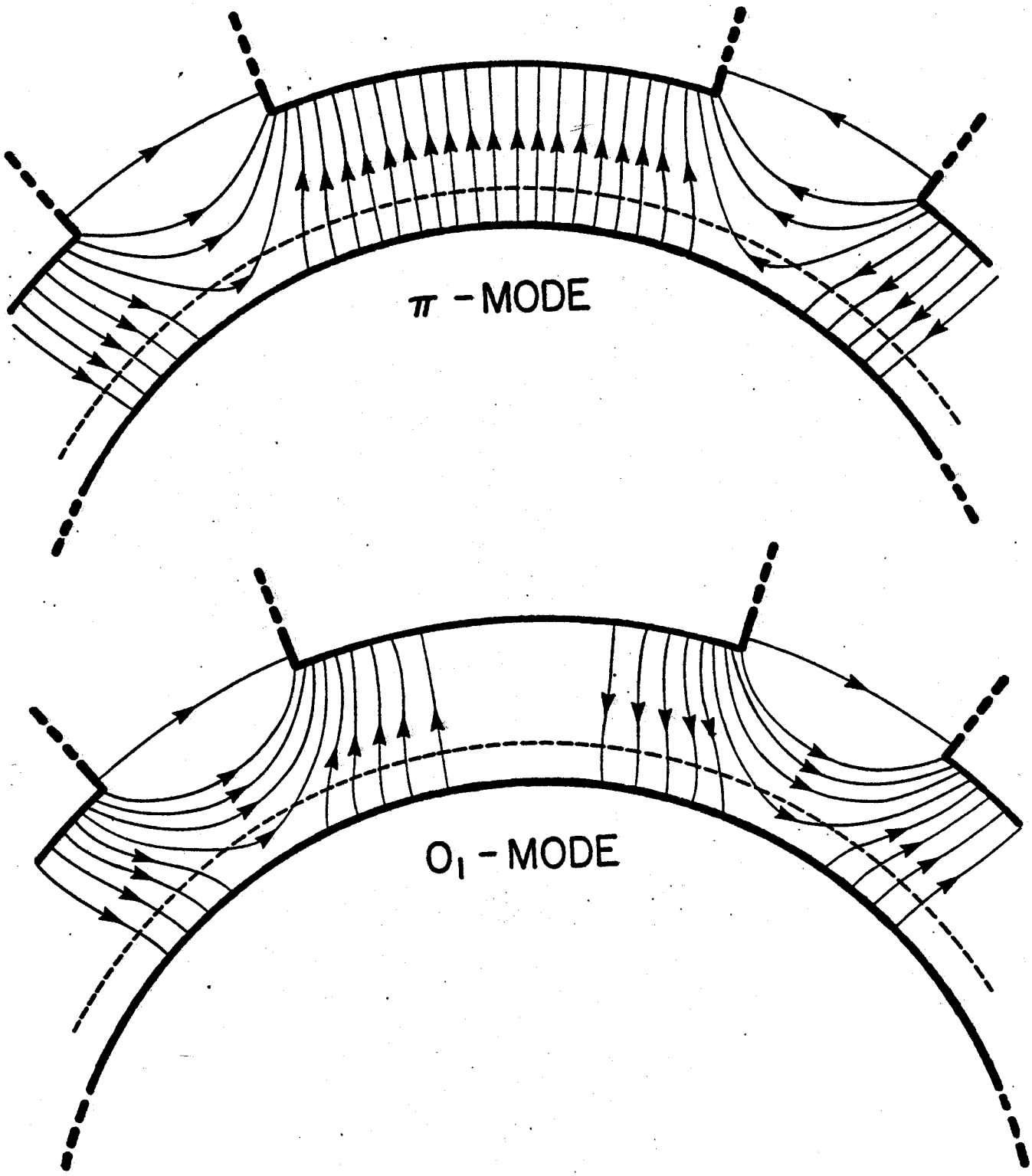

Fig.5

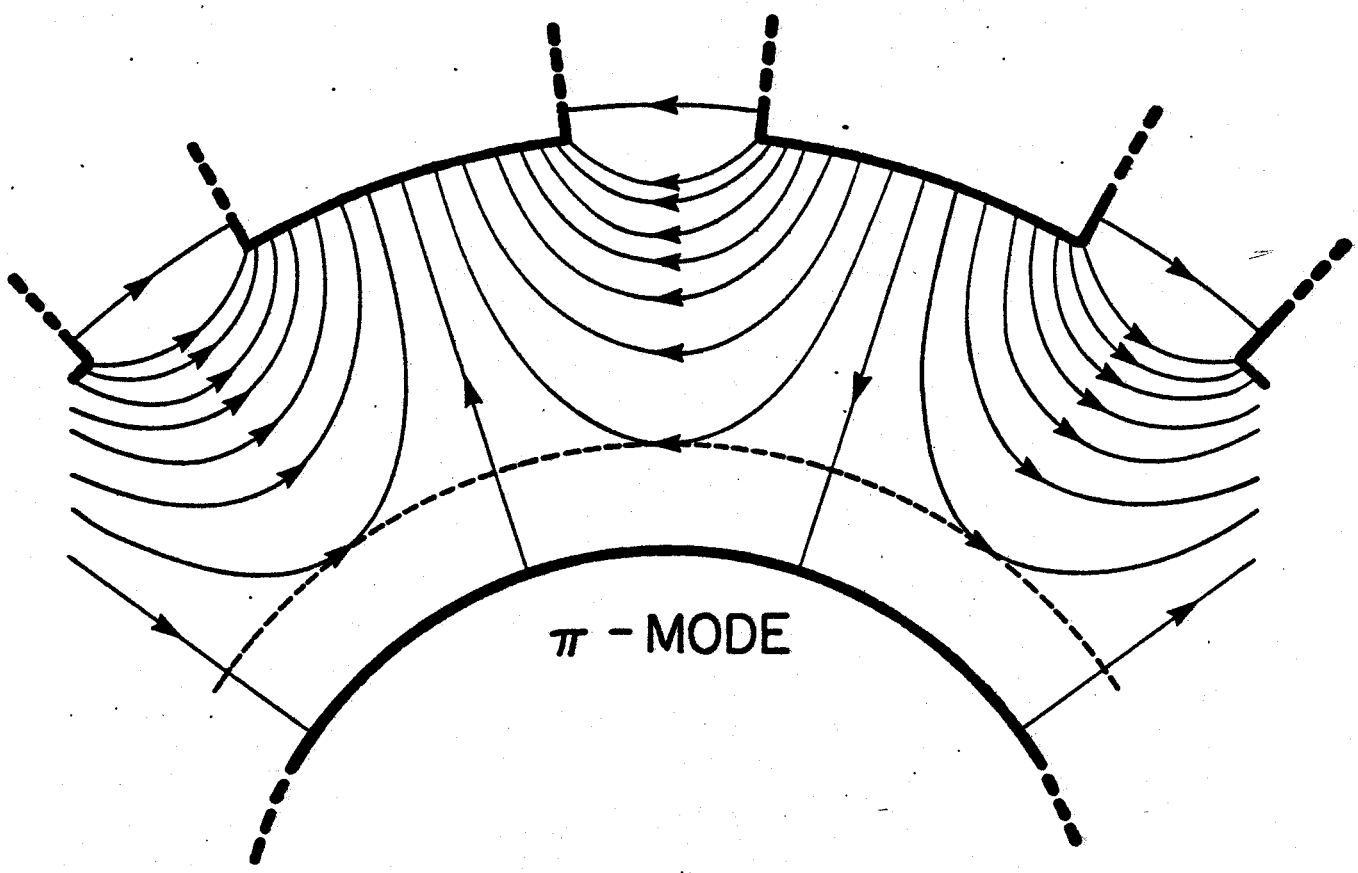

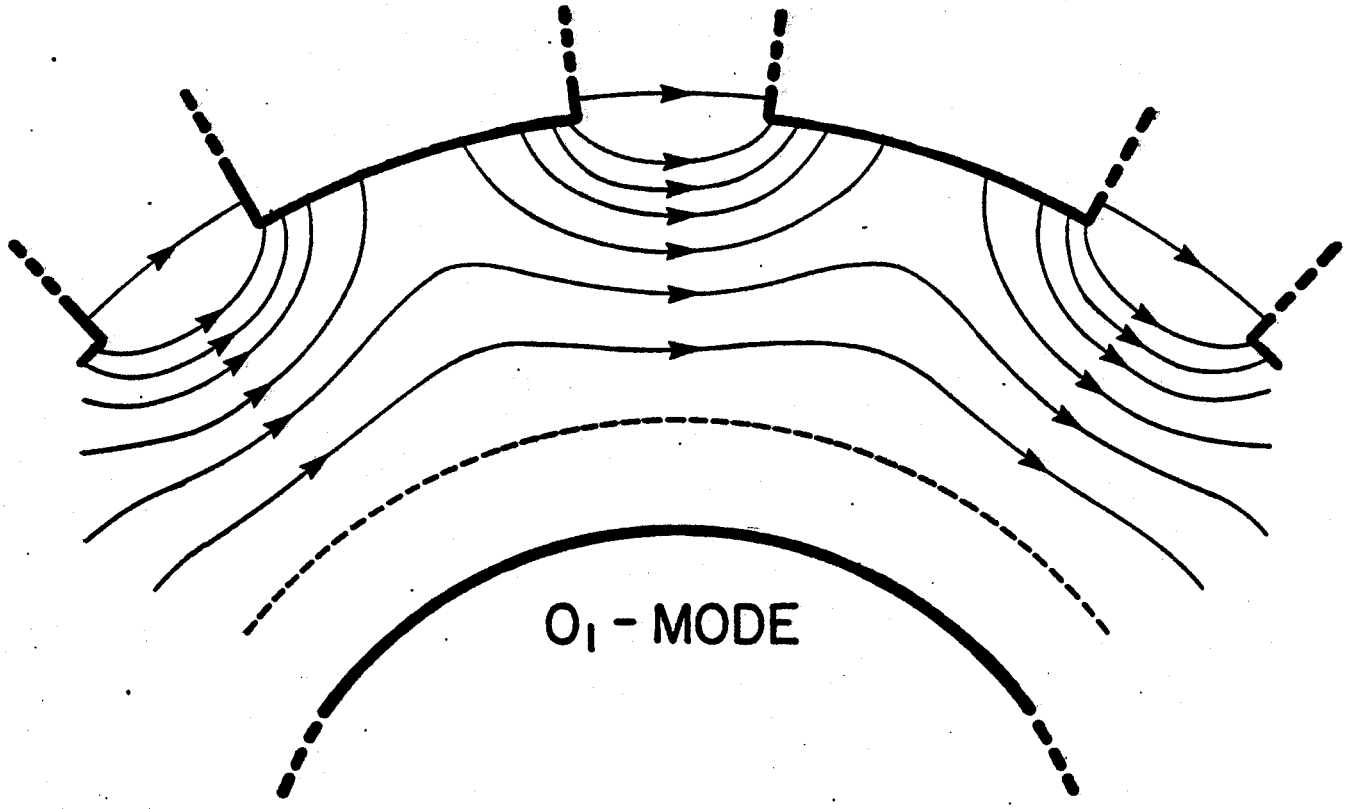

Fig.6

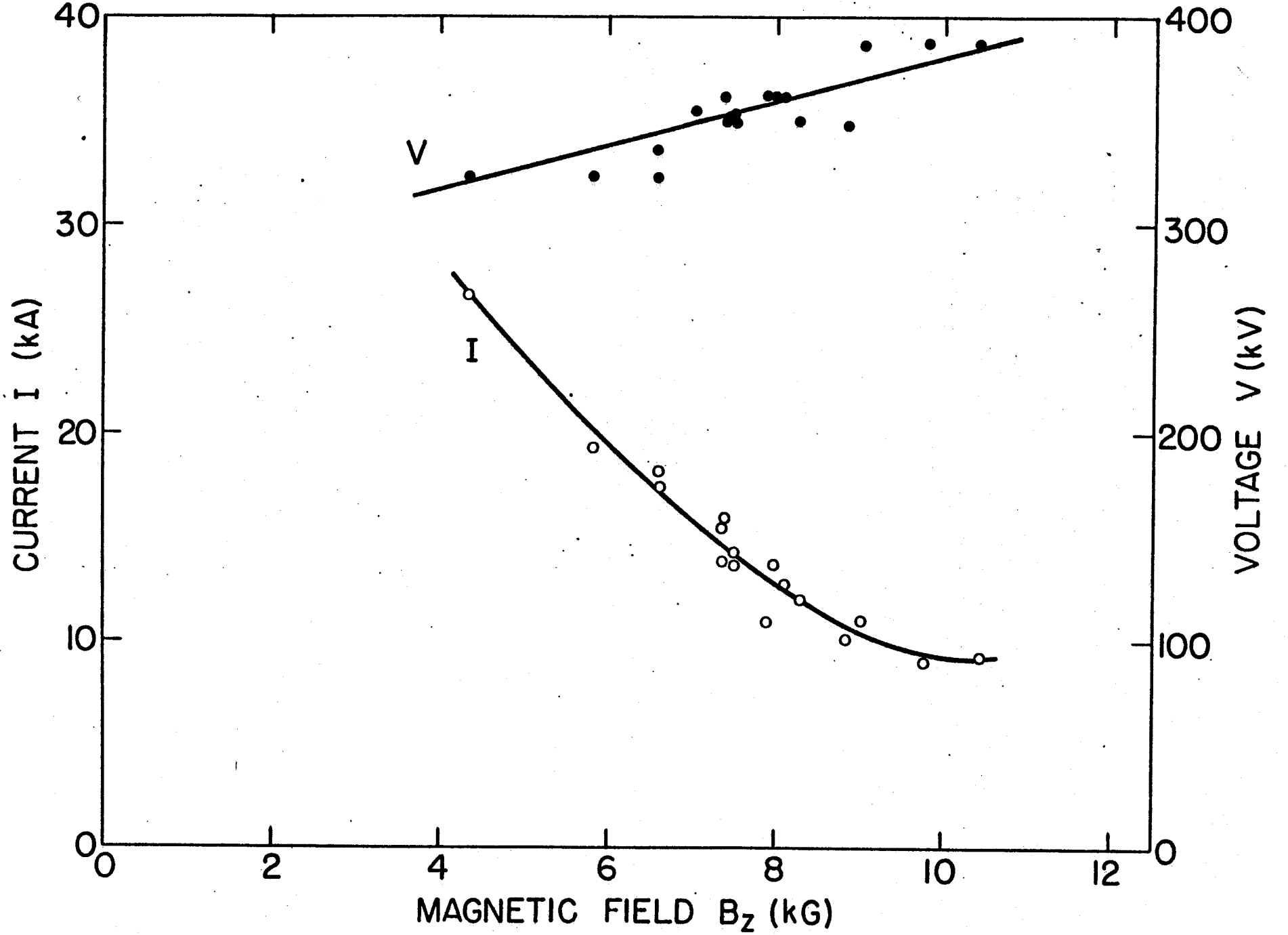
40
30
20
10
0
400
300
200
100
0
0
2
4
6
8
10
12
V
I
CURRENT I (kA)
VOLTAGE V (kV)
MAGNETIC FIELD B_z (kG)

Fig.7

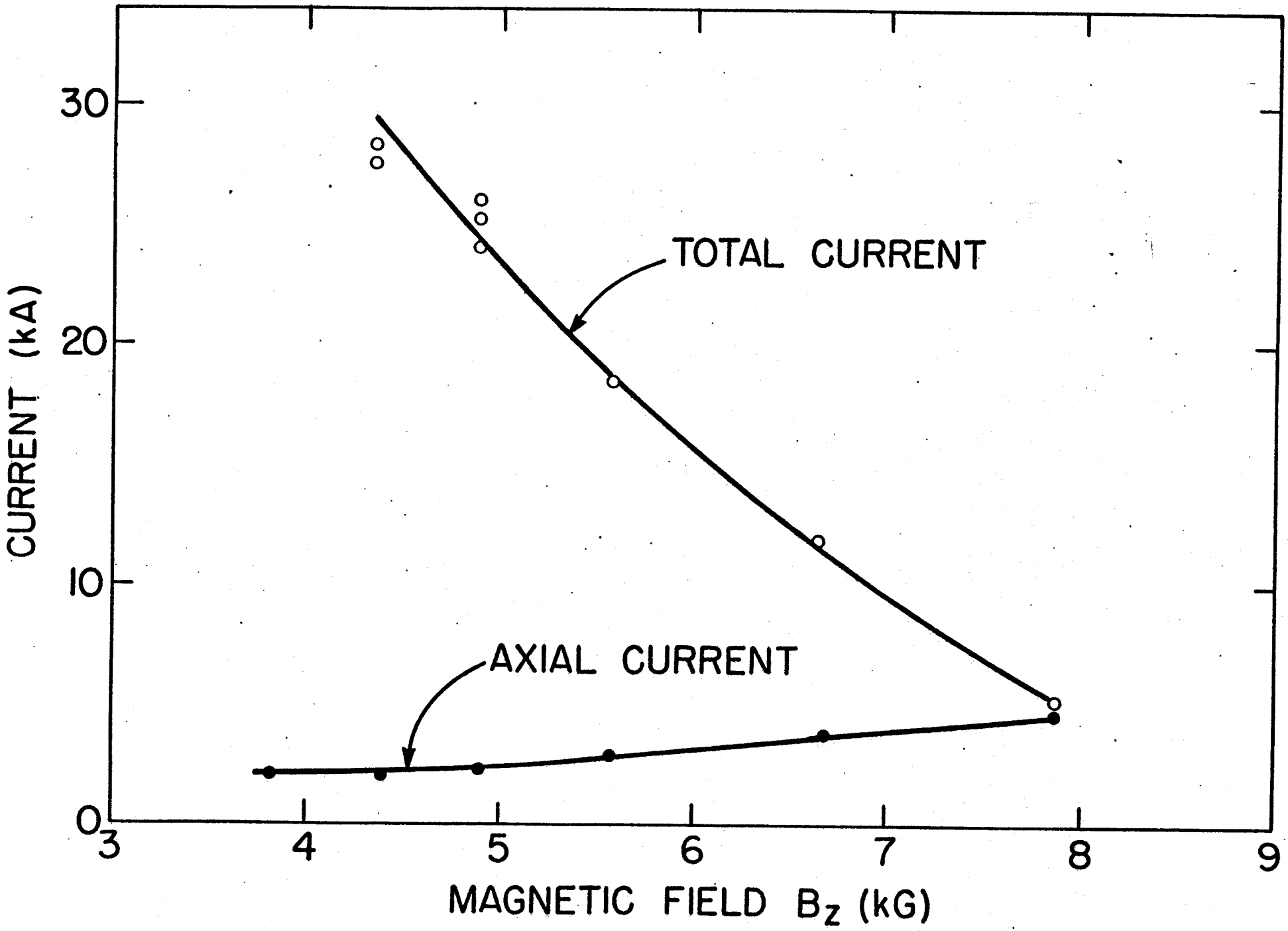

Fig.8
Palevsky and Bekefi

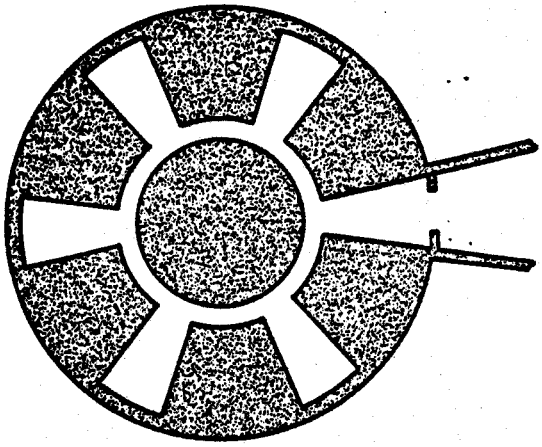

(a)

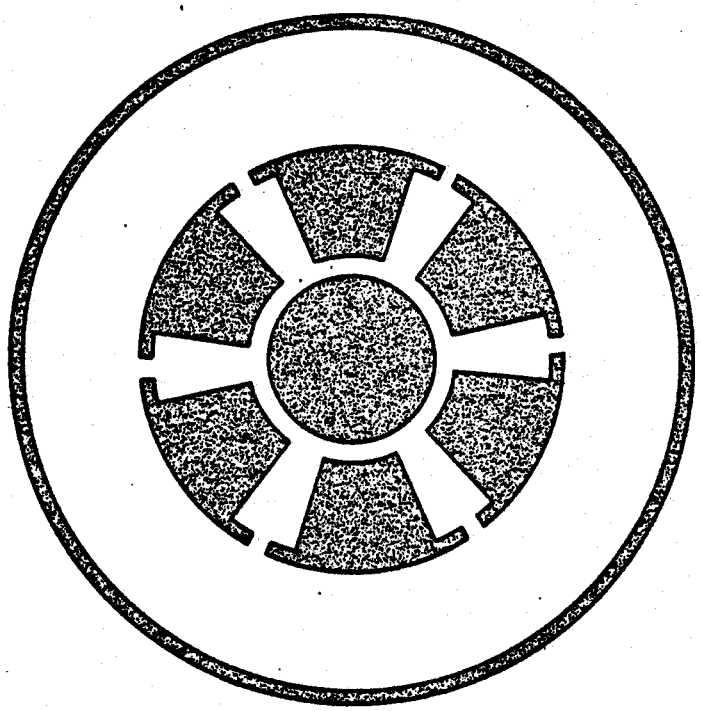

(b)

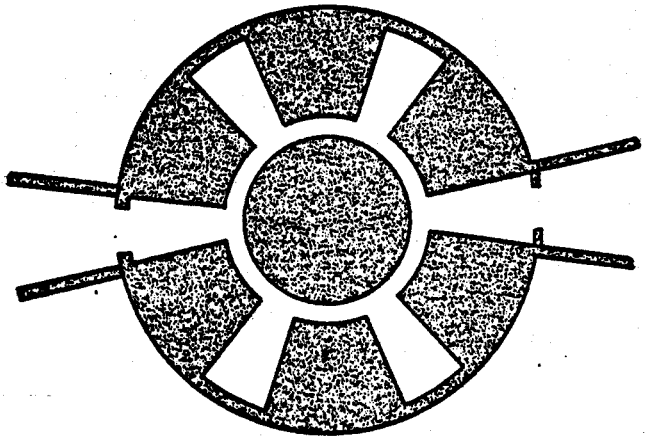

(c)

Fig.9

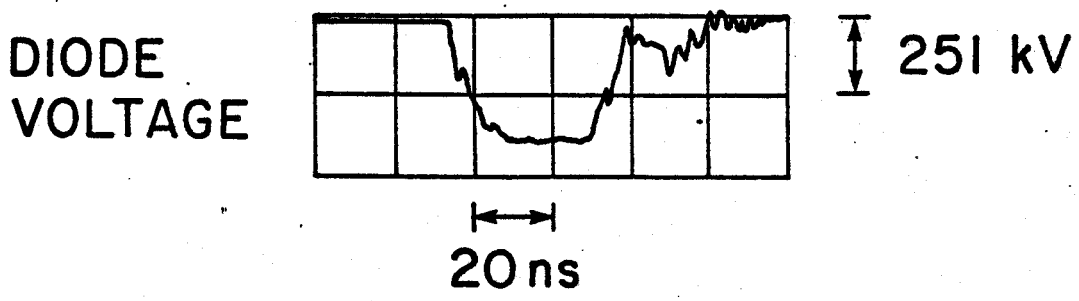
DIODE
VOLTAGE
251 kV
20 ns

(a)

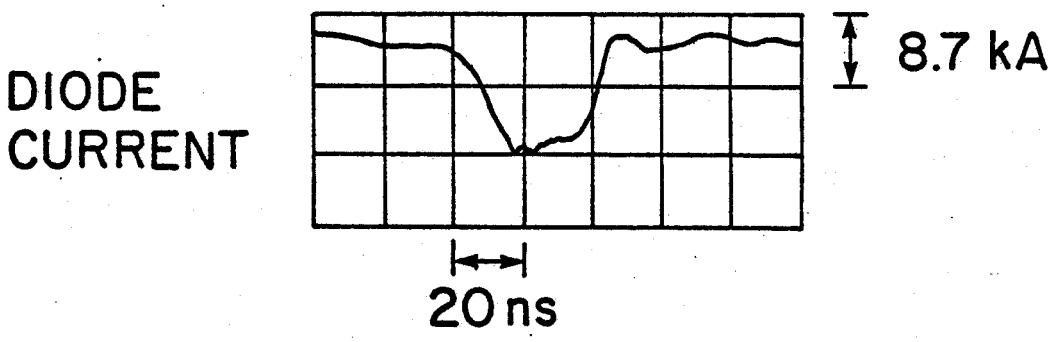
DIODE
CURRENT
8.7 kA
20 ns

(b)

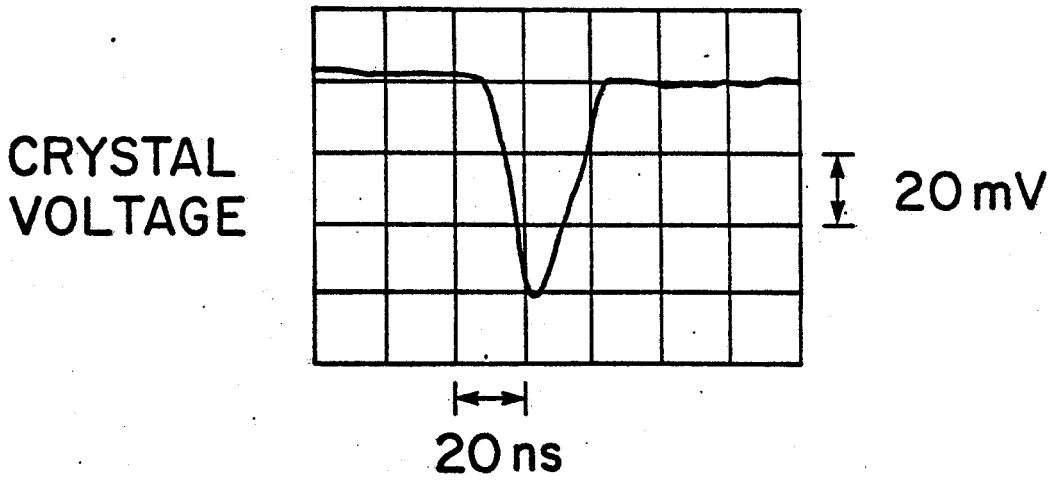
CRYSTAL
VOLTAGE
20 mV
20 ns

(c)

Fig.10

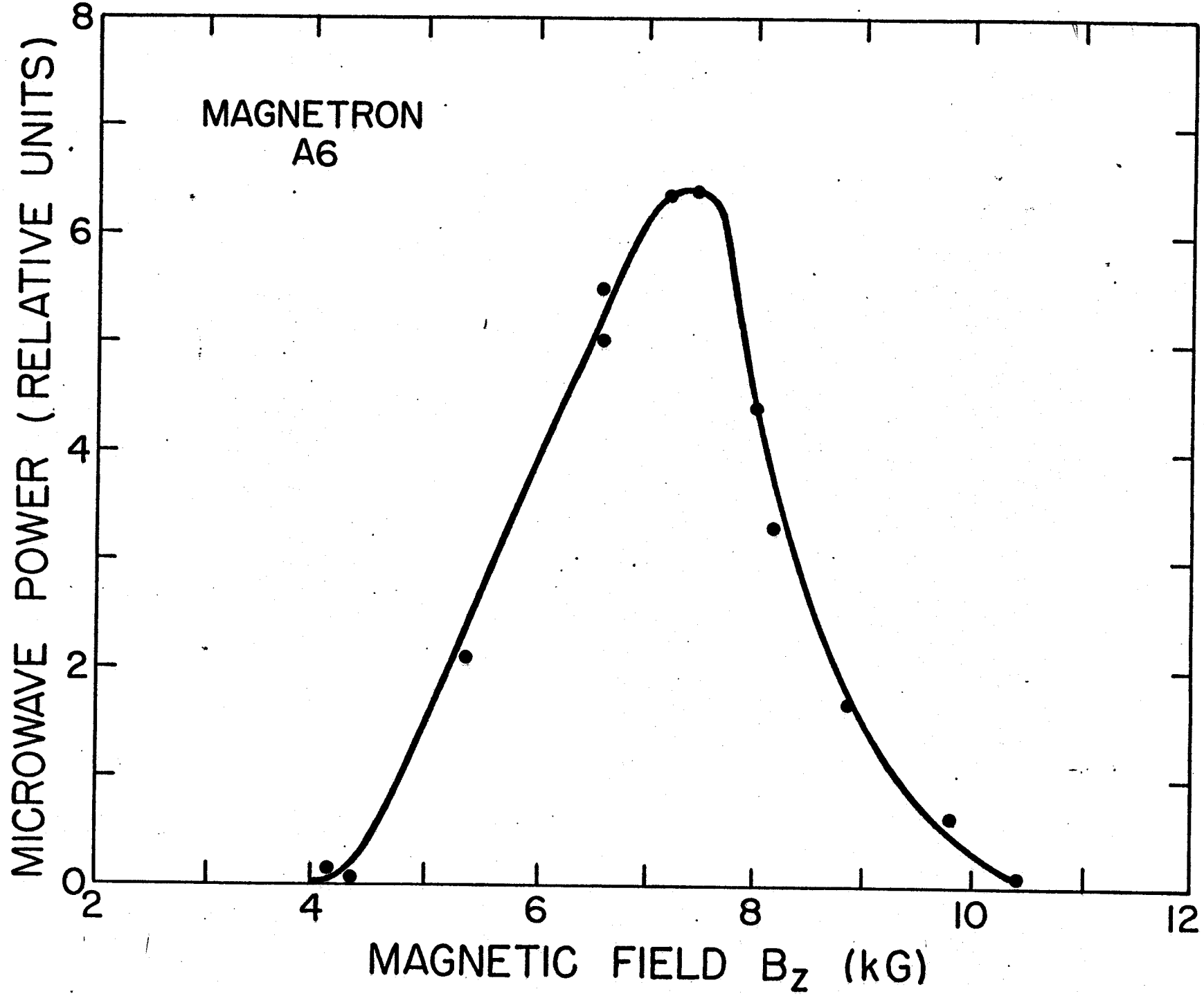
MAGNETRON
A6
MICROWAVE POWER (RELATIVE UNITS)
0
2
4
6
8
2
4
6
8
10
12
MAGNETIC FIELD B_z (kG)

Fig. 11

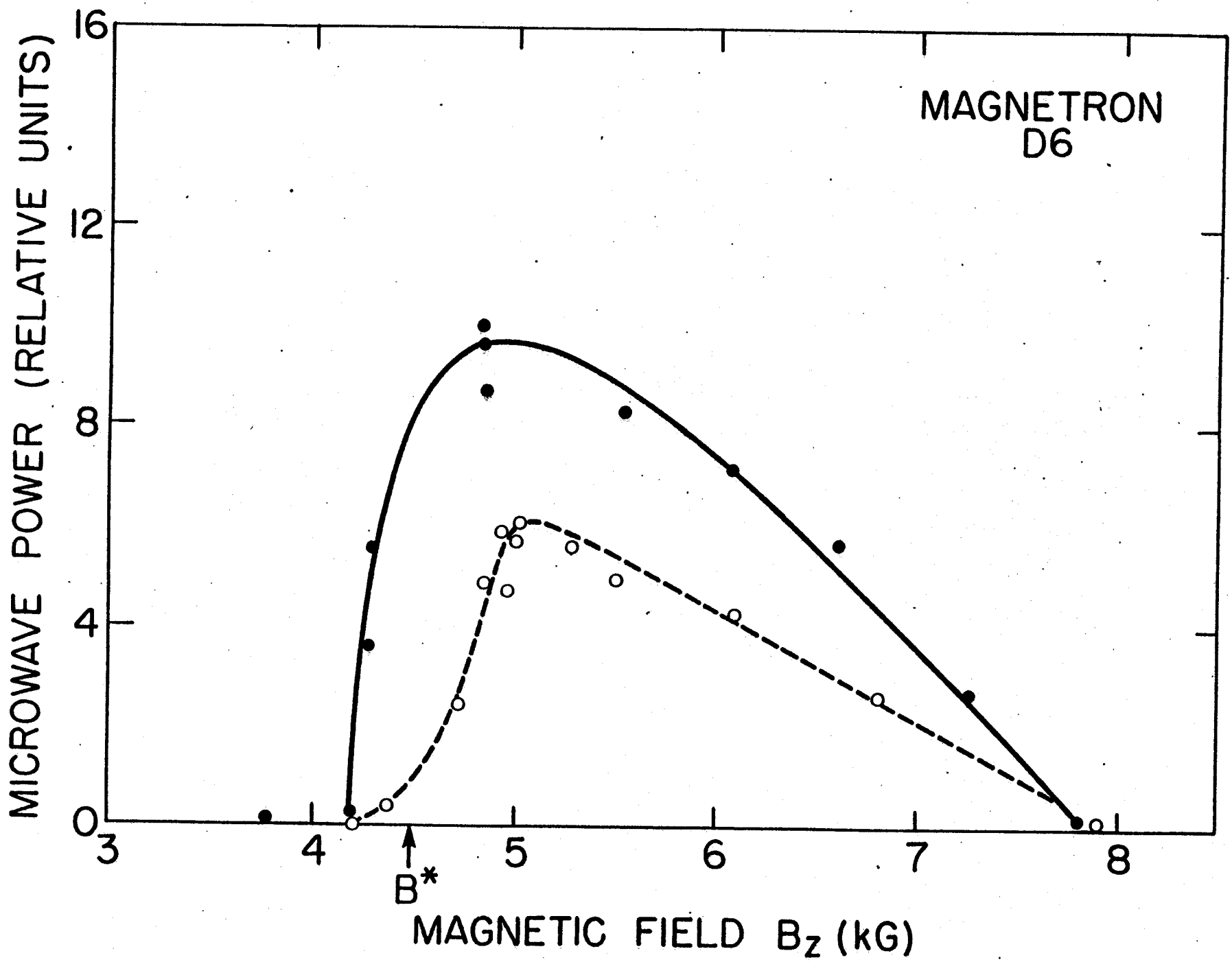
MAGNETRON
D6
MICROWAVE POWER (RELATIVE UNITS)
16
12
8
4
0
3
4
5
6
7
8
B*
MAGNETIC FIELD B_z (kG)

Fig. 12

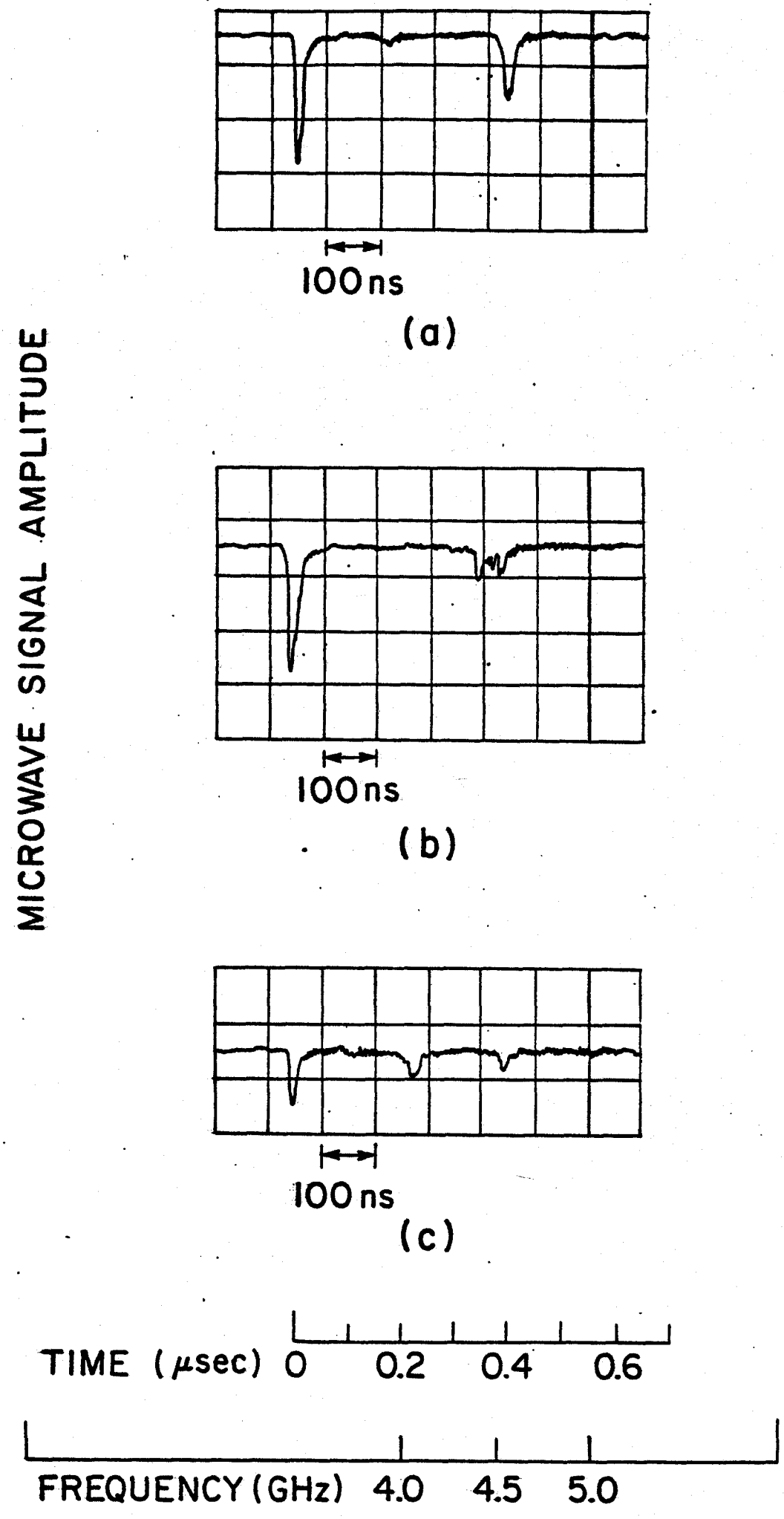
100 ns
(a)
MICROWAVE SIGNAL AMPLITUDE
100 ns
(b)
100 ns
(c)
TIME (μsec) 0 0.2 0.4 0.6
FREQUENCY (GHz) 4.0 4.5 5.0

Fig. 13

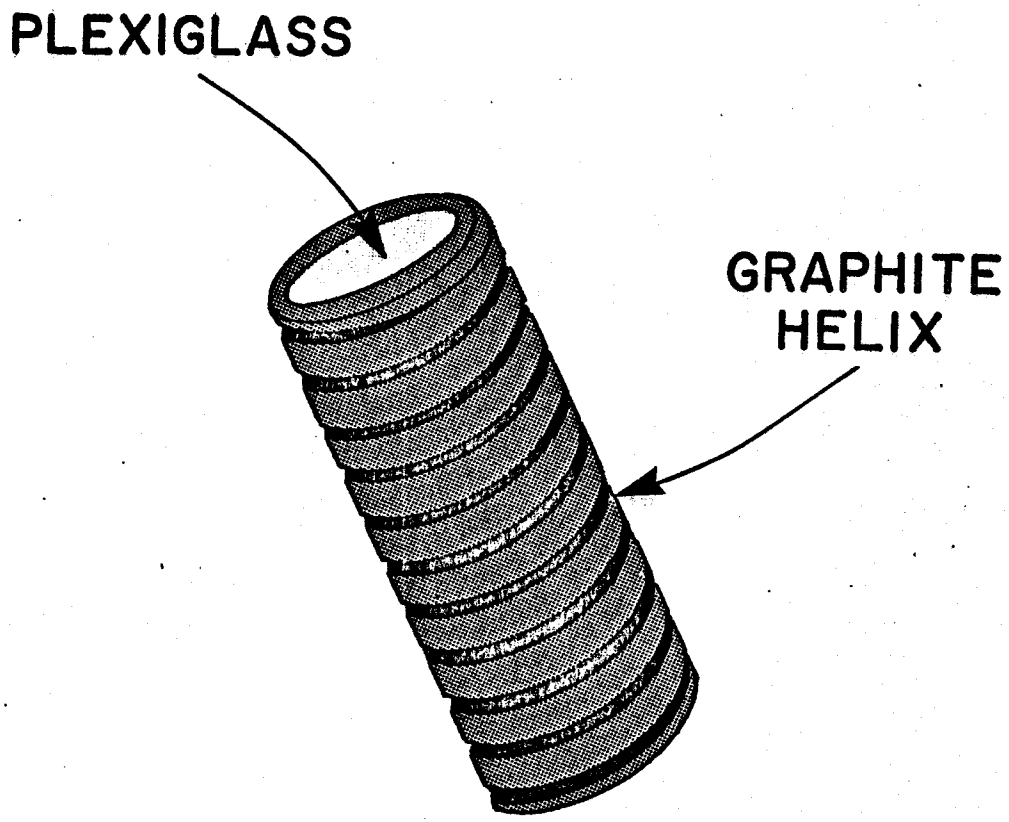

Fig. 14
Palevsky and Bekefi